Simulating the Effect of Cell Migration Speed on Wound Healing Using a 3D Cellular Automata Model for Multicellular Tissue Growth

Belgacem Ben Youssef(✉)

Department of Computer Engineering, College of Computer and Information Sciences, King Saud University, Riyadh, Saudi Arabia
BBenyoussef@ksu.edu.sa

Abstract. We present the simulation of the effect of cell migration speed on wound healing using a three-dimensional computational model for multicellular tissue growth. The computational model uses a discrete approach based on cellular automata to simulate wound-healing times and tissue growth rates of multiple populations of proliferating and migrating cells. Each population of cells has its own division, motion, collision, and aggregation characteristics resulting in a number of useful system parameters that allow us to investigate their emergent effects. Our sequential performance results point to the need of porting the model to modern high performance machines to harness the computational power available in multicore and GPU-based computers. Discrete systems of this kind can be a valuable approach for studying many complex systems, including biological ones.

Keywords: Cellular automata · 3D model · Tissue growth · Wound healing · Cell migration

1 Introduction

Cell motility is important for the proliferation of mammalian cells. In addition, it is paramount in many physiological processes such as angiogenesis, wound healing, inflammation, and tumor cell metastasis [1]. Increased motility of cells significantly enhances their proliferation rates, and thus directly affects the population dynamics of tissue growth. The structure of natural tissues is supported by an extracellular matrix (ECM) that has the form of a three-dimensional network of cross-linked protein strands (see Figure 1, for an example). The ECM plays many important roles in tissue development. Biochemical and biophysical signals from the ECM modulate fundamental cellular activities, including adhesion, migration, proliferation, differentiation, and programmed cell death [3]. Scaffold properties, cell activities like adhesion or migration, and external stimuli that modulate cellular functions are among the many factors that affect the growth rate of tissues [4].

O. Gervasi et al. (Eds.): ICCSA 2015, Part II, LNCS 9156, pp. 28–42, 2015.
DOI: 10.1007/978-3-319-21407-8_3

As a result, the development of bio-artificial tissue substitutes involves extensive and time-consuming experimentation. The development of computational models with predictive abilities could enhance progress in this area. In this context, the simulation of the effect of cell migration under different conditions is necessary to evaluate their charactersitics, screen many alternatives, and choose only the most promising ones for laboratory experimentation.

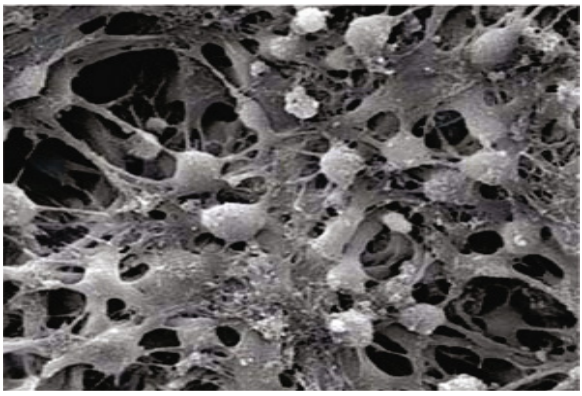

Fig. 1. A scanning electron micrograph displaying the three-dimensional structure of an extracellular matrix

This research describes a three-dimensional cellular automata (CA) model to simulate the growth of three-dimensional tissues consisting of more than one cell type in a wound-healing environment. The corresponding discrete model is an extension of a previously developed base model that accounted for only a single type of cells [5]. The model incorporates all the elementary features of cell division and locomotion including the complicated dynamic phenomena occurring when cells collide and aggregate. Each computational element is represented by a site within a cubic lattice. While the assumption of cubic living cells does not reflect the true morphology of migrating or confluent mammalian cells, it allows us to use data structures that minimize memory and computational time requirements. Here, each computational site interacts with its neighbors that are to its north, east, west, south, and immediately above it or below it. This is known as the von Neumann neighborhood in three dimensions [6]. Our objective is to evaluate the effects of cell migration speed on the tissue growth rate and wound-healing time in the context of a mixed wound-seeding topology employing two types of cell populations. In particular, we explore the following question:

– What are the effects of cell migration speed on the wound-healing time and tissue growth rate?

In the next section, we define the concept of cellular automata. This is followed by a concise review of related work and a short description of the development of the model. We then present the corresponding sequential algorithm and include its flowcharts. Before concluding, we give an overview of the important parameters and inputs of the model and discuss our performance and simulation results.

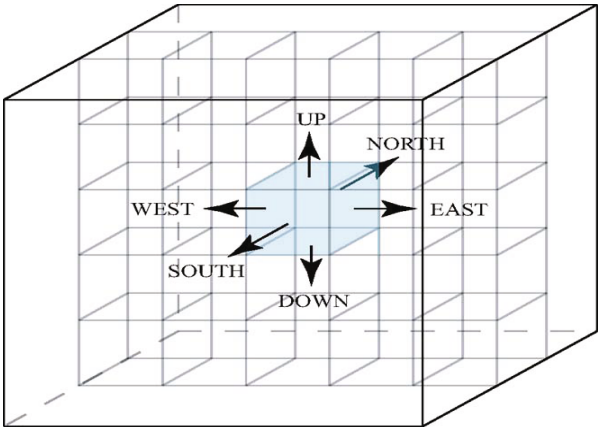

Fig. 2. The von Neumann neighborhood in three dimensions used in our CA model

2 Cellular Automata Concepts

Cellular automata were originally introduced by John von Neumann and Stanislaw Ulam as a possible idealization of biological systems with a particular purpose of modeling biological self-reproduction [7]. This approach has been used since then to study a wide variety of physical, chemical, biological, and other complex natural systems [7].

We consider d-dimensional cellular automata consisting of an array D of lattice cells covering a finite domain. Any cell c is uniquely identified by d integer coordinates $(i_1, i_2, \ldots, i_d)$, where $1 \leq i_1 \leq N_1$, $1 \leq i_2 \leq N_2$, ..., and $1 \leq i_d \leq N_d$. Let Ω be the set of all computational sites in the cellular space and N be the total number of such sites such that $N = N_1 \times N_2 \times \ldots \times N_d$. A cellular automaton satisfies the following properties:

1. Each cell c interacts only with its neighbor cells defined by a neighborhood relation that associates with the cell c a finite list of neighbor cells $c+\nu_1, c+\nu_2, \ldots, c+\nu_k$. In general, the neighborhood vector (or neighborhood index), $V = [\nu_1, \nu_2, \ldots, \nu_k]$, may vary from one cell to another.
2. Each cell can exist in one of a finite number of states. This finite list of states will be listed by Q. In the simplest case of two-state automata, $Q = \{0, 1\}$.
3. Each function $X : \Omega \longrightarrow Q$ defining an assignment of states to all cells in the cellular space Ω is called a configuration. Then, x_c is called the state of the cell c under configuration X.
4. For any cell c in the cellular space, there exists a local transition function (or rule) f_c, from Q^k to Q, specifying the state of the cell at time level $t+1$ as a function of the states of its neighbors at time level t. That is, $x_c^{t+1} = q^{t+1}(c) = f_c(x^t_{c+\nu_1}, x^t_{c+\nu_2}, \ldots, x^t_{c+\nu_k})$.
5. The simultaneous application of the local transition functions f_c to all the cells in a cellular space defines a global transition function F which acts on

the entire array transforming any configuration X^t to a new configuration X^{t+1} according to $X^{t+1} = F(X^t)$.

These properties imply that each cellular automaton is a discrete dynamical system. Starting from an initial configuration X^0, the cellular array follows a trajectory of configurations defined by the global transition function F. All possible configurations of the cellular automaton define a set Φ, whose cardinality can be quite large. For instance, using $N_1 = N_2 = N_3 = 5$ and $Q = \{0, 1\}$, the number of configurations in Φ would be equal to $2^{5\times5\times5} \approx 4.254 \times 10^{37}$ configurations.

We can now define parallel discrete iterations for a cellular automaton as follows:

$$\begin{cases} X^0 & \text{is given in } \Phi \\ X^{t+1} = F(X^t), \end{cases} \tag{1}$$

for $t = 0, 1, 2, \ldots$ or equivalently:

$$\begin{cases} X^0 & = (x_1^0, x_2^0, \ldots . x_N^0) \text{ is given in } \Phi \\ X_f^{t+1} & = f_i(x_1^t, x_2^t, \ldots, x_N^t), \end{cases} \tag{2}$$

for $t = 0, 1, 2, \ldots$ and $i = 1, 2, 3, \ldots, N$. The preceding two equations, or rules, imply that the parallel discrete iterations update the states of all cells at the same time. It should be noted here that the transition functions of cellular automata need not be algebraic in form and may be rule-based. A potentially important feature of cellular automata is the capability for *self-reproduction* through which the evolution of a configuration yields several separated, yet identical copies of the configuration. Moreover, cellular automata rules may map several initial configurations into the same final configuration, thus leading to microscopically *irreversible* time evolution in which trajectories of different states may merge [8].

3 Related Work

Various modeling approaches have been used to simulate the population dynamics of proliferating cells. These models can be classified as: deterministic, stochastic, or based on cellular automata and agents. We briefly review a few of the recent cellular automata and agent-based lattice-free models to simulate tissue growth. Chang and his team developed a 3-D cellular automata based model to describe the growth of microbial cell units [9]. This model considered the effects of bacterial cell division and cell death. Other CA-based models have also been used to solve more specific biological modeling problems. For instance, Kansal et al. developed a model to simulate brain tumor growth dynamics [10]. Their model utilizes a few automaton cells to represent thousands of real cells, thus reducing the computational time requirements of the model while limiting its ability to track individual cells in the cellular space. Another CA model was used by Cickovski et al. as a framework to simulate morphogenesis [11]. This model used a hybrid approach to simulate the growth of an avian limb. The

cellular automaton governed cell interactions while reaction-diffusion equation solvers were used to determine the concentration levels of surrounding chemicals.

Some of the agent-based models apply the dynamics of cell proliferation and death to describe tissue pattern formation and growth [12]. Other related models are suitable for describing the locomotion of a fixed number of cells where cells move relatively slowly with respect to other processes like the diffusion of soluble substances [13]. Additional models employ feedback mechanisms between cells and the substrate to model cells entering and leaving the tissue and to establish homeostasis in such systems [14]. Some of the agent-based models use regular triangulation to generate the neighborhood topology for the cells, thus allowing for a continuous representation of cell sizes and locations in contrast to grid-based models [15]. Others utilize multiscale approaches to model collective phenomena in multicellular assemblies, including inflammation and wound healing [16].

4 The Computational Model

The growth of tissues is a complex biological process. In this model, the migration and proliferation of mammalian cells are considered to be mainly characterized by the following four subprocesses: cell division, cell motion, cell collision, and cell aggregation. For a detailed account of the modeling steps of each of these subprocesses, we refer the reader to related reference [5].

4.1 States of the Cellular Automaton

The model is a discrete system operating in a cellular space containing $N = N_x \times N_y \times N_z$ computational sites. Cells in the cellular space interact with their neighbors at equally spaced time intervals $t_1, t_2, \ldots, t_r, t_{r+1}, \ldots$ where $t_{r+1} = t_r + \Delta t$ for all r. An occupied computational site must describe the current state of a given cell using a set of values. These values must describe the asynchronous proliferation and persistent random walks of multiple cell types. In building an adequate state definition, sufficient information must be provided about the history so that given the current state, the past is statistically irrelevant for predicting all future behavior pertinent to the application at hand [17]. Based on these specifications, the state x_i of an automaton containing a living cell must specify the following set of parameters:

1. The cell type.
2. The direction of cell motion.
3. The cell speed.
4. The time remaining until the next direction change.
5. The time remaining until the next cell division.

The average speed of migrating cells is controlled by varying the value of the time interval, . This is due to the fact that migrating cells cover a fixed distance in each step. Another means of regulating the speed of locomotion is the

ability to adjust the transition probability for the stationary state. Therefore, a migrating cell of type j in automaton i must only specify the direction of locomotion and the times which remain until the next direction change and the next cell division in its state x_i. The state of an arbitrary automaton i, thus, takes values from the following set of eight-digit integer numbers $\Psi = \{klmnpqrs/k, l, m, n, p, q, r, \text{and } s \in \mathbb{N}\}$, where k is the cell type. The direction of motion is identified by the direction index l. When l is equal to 0, the cell is in the collision stationary state. When the value of l is in the range of 1 to 6, it represents one of six directions the cell is currently moving in. When the value of l is 7, it enters an aggregation stationary state where it "sticks" to another cell of the same type potentially forming cellular aggregates. The digits mn denote the persistence counter. This counter represents the time remaining until the next change in the direction of cell movement. The cell phase counter is given by the remaining four digits $pqrs$ and holds the time remaining before the cell divides.

5 Sequential Algorithm

5.1 Initial Conditions

The initial parameters for the simulation are first read from the input data file. Then, the computational sites to be occupied by the cells at the start of this simulation run are selected based on the seeding mode of the initial cell distribution. For each occupied site, we assign a cell state based on the population characteristics of that cell type. The direction index is randomly selected, the persistence counter is assigned a properly chosen value, and the cell phase counter is set based on experimentally determined cell division data.

5.2 Iterative Operations

At each time step $t_{r+1} = t_r + \Delta t$, for $r = 0, 1, 2, \ldots$

1. Randomly select a computational site.
2. If this site is occupied by a cell c and the phase counter is zero then it is time for this cell to divide and the division routine is called.
3. If this site is occupied by a cell c and the persistence counter is zero, then it is time for this cell to change directions and the direction change routine is called.
4. If this site is occupied by a cell c and both the phase and persistence counters are not zero, attempt to move this cell to a neighboring site in the direction indicated by the direction index of its current state.
   (a) If this neighboring site is free, then mark it for cell c and decrement the phase and persistence counters by one.
   (b) If this neighboring site is occupied by a cell from a different type, then cell c remains in the current site and both cells enter the stationary state due to collision. Their persistence counters are set accordingly while their respective phase counters are decremented by one.

(c) If this neighboring site is occupied by a cell from the same type, then cell c remains in the current site and both cells enter the aggregation stationary state. The persistence counters for both cells are set to the appropriate waiting time and their phase counters are decremented by one.

5. Select another site (randomly) and repeat Steps 2-4 until all sites have been processed.
6. Update the states of all sites so that the new locations of all cells are computed.
7. If confluence has not been reached, proceed to the next time step.

The flowcharts of the main module of the sequential algorithm and those of the division and direction change routines are displayed in figures 3 through 6, respectively.

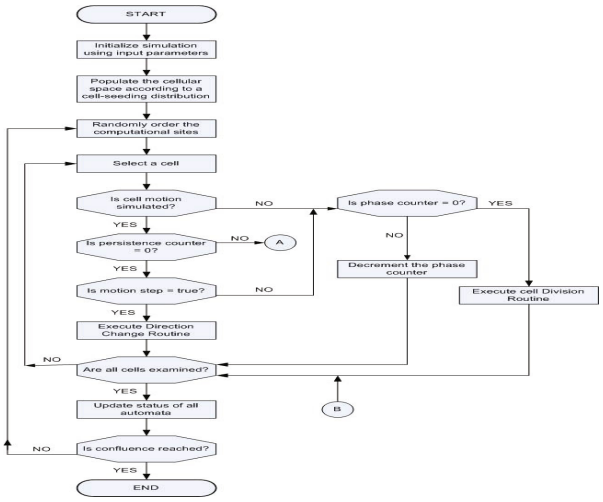

Fig. 3. Flowchart of the main module of the sequential algorithm (part 1 of 2)

6 Simulation Parameters for Wound Healing

6.1 Cell Seeding Distribution

In this study, we consider a wound-seeding topology where a wound in the shape of an empty cylinder is centered in the cellular grid with all surrounding sites occupied by two types of cells. This topology simulates the cell migration and proliferation phase of wound healing. This model does not attempt to describe all the steps of the complicated wound-healing process [18]. We associate one type of cell distributions with this seeding topology, known as the mixed distribution. All cell

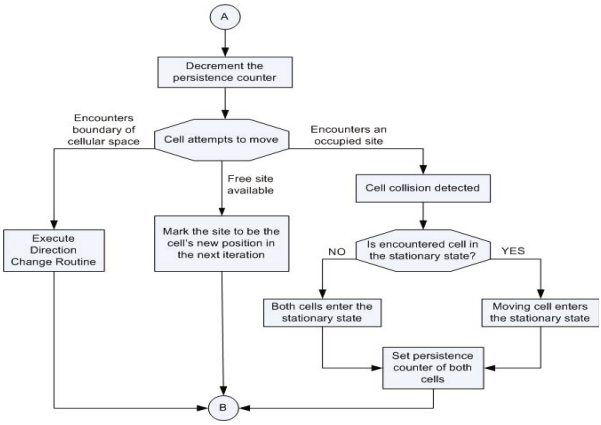

Fig. 4. Continuation of the flowchart of the main module (part 2 of 2)

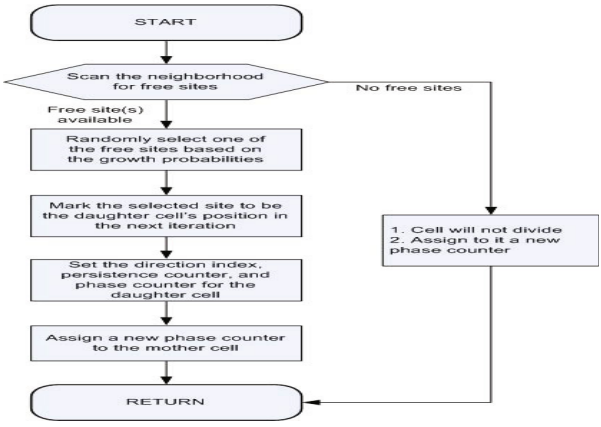

Fig. 5. Flowchart showing the cell division routine

types are seeded together in all areas surrounding the denuded area of the wound environment using a uniformly random placement of cells. During the simulation, cells of both types can migrate freely in the wound area. Figure 7 illustrates an example of this seeding distribution.

6.2 Cell Population Dynamics

Starting with a total number of seed cells equal to N_0, the CA rules transform the cellular array to simulate the dynamic process of tissue growth inside the wound environment. At some time t after the start of the simulation, $N_c(t)$ sites of the cellular automaton are occupied by cells. We define a measure to indicate the volume coverage at time t inside the wound area as the cell volume fraction $k(t)$, as follows:

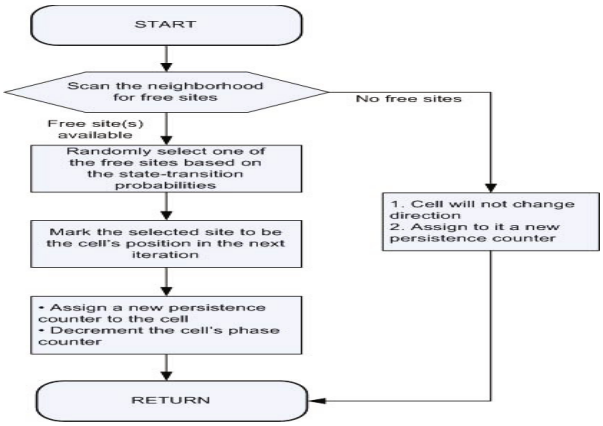

Fig. 6. Flowchart depicting the direction change routine

$$k(t) = \frac{N_c(t) - N_0}{N - N_0} = \frac{\sum_{i=1}^{n} (N_{c_i}(t) - N_{c_i}(0))}{N - \sum_{i=1}^{n} N_{c_i}(0)} ,$$

with $N_0 = N_c(0) = \sum_{i=1}^{n} N_{c_i}(0)$ and where $N(= N_x \times N_y \times N_z)$ is the size of the cellular space, $N_{c_i}(t)$ is the number of occupied computational sites by cell type i at time t, $N_{c_i}(0)$ is the number of seed cells of type i surrounding the wound, and n is the number of cell types ($n \geq 1$). For the wound seeding, the cell volume fraction indicates the fraction of cells occupying the wound area at a given time. Thus, the time to reach full volume coverage can be an approximation to the wound-healing time, an important parameter in wound healing research.

The overall tissue growth rate represents the increase in volume coverage, within the wound area, with respect to time. To this end, the tissue growth rate measure is given by the following formula:

$$\frac{dk(t)}{dt} = \frac{\sum_{i=1}^{n} (N_{c_i}(t) - N_{c_i}(t - \Delta t))}{\Delta t \times (N - N_0)} = \frac{\sum_{i=1}^{n} (N_{c_i}(t) - N_{c_i}(t - \Delta t))}{\Delta t \times (N - \sum_{i=1}^{n} N_{c_i}(0))} .$$

Here, $k(t)$ is the cell volume fraction at time t as given above and Δt is the time step in hours or days, depending on the resolution of the time scale utilized in the model. The simulation continues until all sites are occupied by cells, that is until $k(t)$ equals one. The movement of cells will slow down due to breaks in the persistent random walks, cell collisions, and cell aggregations. Thus, only a fraction of the total cells, $N_c(t)$, will move in the time interval $[t,\ t + \Delta t]$ and

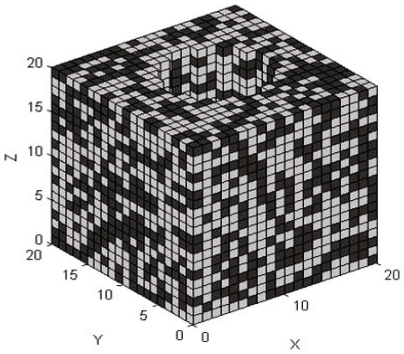

Fig. 7. An example of a mixed wound-seeding topology, comprised of two types of cell populations, is depicted. A wound of cylindrical shape, with a diameter of 10 and a height of 20, inside a $20 \times 20 \times 20$ cellular grid is exhibited.

the effective speed of migration, $S_e(t)$, in a wound-seeding environment can be computed by using the following equation:

$$S_e(t) = \frac{N_m(t)}{N_{c,w}(t)} \times S \,, \tag{3}$$

where $N_m(t)$ refers to the number of moving cells in the time interval $[t,\ t+\Delta t]$, $N_{c,w}(t)$ is the number of occupied sites inside the wound area at time t, and S is the individual cell "swimming" speed. We also define the cell heterogeneity measure H as the ratio of the initially seeded number of cells from population 1 to that from population 2. This is given by:

$$H = \frac{\text{initial number of (faster) cells from population 1}}{\text{initial number of (slower) cells from population 2}} \,.$$

That is, when $H = 9$ there are 9 cells from population 1 for every cell from population 2.

6.3 Additional Simulation Inputs

The simulation results of the proliferation of multiple cell types are obtained for a $200 \times 200 \times 200$ cellular array where two cell populations are used with a wound diameter of 100 and a height of 200. A confluence parameter of 100%, an average waiting time of 2 hours for the six directions of motion and 1 hour for the two stationary states are utilized. The cell speed of population 1 is assigned values of $1, 2, 5, 10,$ and $50\mu m$ per hour while the speed of migration of cells in population 2 is kept constant at $1\mu m$ per hour. In addition, a cell heterogeneity ratio of $H = 1$ is maintained throughout the simulations so that an equal number of cells from both populations is used to populate the tissue surrounding the wound. Each

cell is modeled as a cubic computational element whose sides are assumed to be equal to $10\mu m$ in length. As given in Table 1, we also employ different division time distributions for these two cell populations.

Table 1. Division time distributions for the two cell populations

	Cell Populations	
Division Times	Cell Population 1	Cell Population 2
12 - 18 hrs	64%	4%
18 - 24 hrs	32%	32%
24 - 30 hrs	4%	64%

6.4 Sequential Performance Results

We implemented the model sequentially on a single node of a high-performance cluster, made available to us by the InfoNetMedia Centre at Simon Fraser University, Canada. Each node uses an Intel P4 3.0-GHz processor with 1 GB of RAM and runs the Gentoo Linux operating system with a GCC compiler version 3.4.4. We compiled the sequential program using the following command: `g++ -O2 -march=pentium4 pro-gram.cpp`. The `-O2` option provides the highest optimization level in the g++ complier without introducing errors into the application while the `-march=pentium4` option instructs the compiler to generate Intel Pentium 4 processor-efficient code.

Due to a limited per-node memory capacity, the largest cellular array size for the sequential runs was $330 \times 330 \times 330$. The following performance results (see Table 2) were obtained for a wound-seeding distribution with a ratio $H = 1$ and cell migration speeds of $10\mu m/hr$ and $1\mu m/hr$ for cell population 1 and cell population 2, respectively. We note that running the model with a large array size is a computationally demanding task that requires small time steps to accurately describe the dynamics of multiple cell populations. In addition to the size of the cellular array, several input parameters affect the execution time needed to run a simulation, including the size of the cylindrical wound, cell migration speed, and cell division time. A simulation using a $200 \times 200 \times 200$ cellular array with a wound diameter of 100 takes $4,059$ seconds (or 1.13 hours) to run serially. Such grid represents a cubical tissue object whose side is only equal to 2 mm and containing a wound with 1 mm in diameter. These performance results point to the need to use parallel computing systems in order to simulate wound healing in the context of multicellular tissues of larger sizes.

7 Simulation Results and Discussion

We discuss our results that simulate the effect of varying the migration speed of cell population 1 on the wound-healing time and tissue growth rate, and then present results that display the temporal evolution of the average speed of all

Table 2. Sequential execution times of the model using different cellular array sizes and wound diameters. The height of the wound is set equal to one dimension of the cellular grid.

Cellular Array	Wound Diameter	Sequential Execution Time (secs)
$150 \times 150 \times 150$	75	1,593
$200 \times 200 \times 200$	100	4,059
$250 \times 250 \times 250$	125	8,536
$300 \times 300 \times 300$	150	15,908
$330 \times 330 \times 330$	165	21,867

cells inside the wound area. Figure 8(a) shows the temporal evolutions of volume coverage as the cell speed of population 1 is varied from $1\mu m/hr$ to $50\mu m/hr$ while cells of population 2 move at a fixed speed of $1\mu m/hr$. A constant cell heterogeneity ratio of $H = 1$ is also maintained in a mixed wound-seeding distribution throughout these simulations. Broadly speaking, we note that volume coverage inside the wound increases with time until it reaches confluence for all values of cell-population-1 speeds. We also observe that as the motility of the cell increases, the proliferation rate increases and hence confluence is attained faster; thus, healing the wound much more quickly (from nearly 24 days to about 5 days). Higher motility of cells decreases the impact of contact inhibition on the proliferation rate as it reduces the formation of cell colonies. Cells moving at increased speeds are the first to enter the denuded wound area seeking to populate its empty sites. This delays the formation of cell colonies and leads to faster proliferation by mitigating the impact of contact inhibition. Furthermore, part (b) of the same figure illustrates the impact of varying the cell speed of population 1 on the overall tissue growth rate. The figure clearly depicts that increasing the cell migration speed leads to higher rates of tissue growth (from a low of about 0.07 to a high of nearly 0.52). Increasing cell migration speeds even to very large values continues to impact positively both the tissue growth rate and the time to reach confluence in the case of this wound-seeding topology. In all simulations, the tissue growth rate increases initially, reaches a maximum and then decreases as a result of contact inhibition brought about by cell-colony formation and merging events that eventually lead to the closure of the wound area and its healing.

Figure 9 depicts the temporal evolution of the effective migration speed, S_e, of all cells in the denuded area of the wound for different cell-population-1 speeds. At the beginning of the simulations, cells move into the wound at their peak speeds. Then, the overall cell speeds drop rapidly as the wound area becomes congested with new daughter cells; and collisions as well as aggregations become more frequent. The average speed decreases with time and shows a drastic decline as confluence is attained due to the formation of local cell clusters and their subsequent mergings.

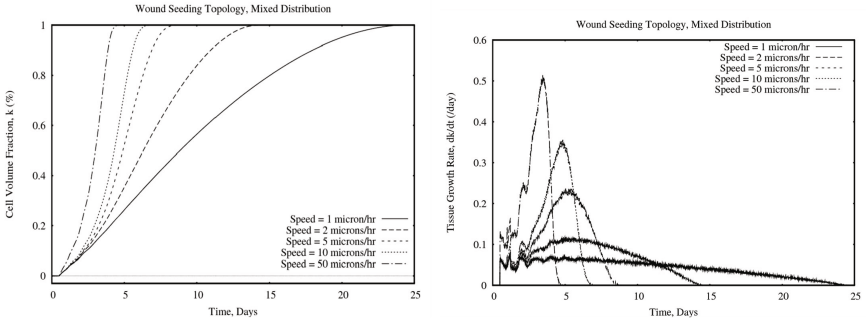

(a) (b)

Fig. 8. The temporal evolution of the (a) cell volume fraction and (b) overall tissue growth rate as the cell speed of population 1 is varied from 1 to $50\mu m/hr$. Cells in population 2 move at a fixed speed of $1\mu m/hr$

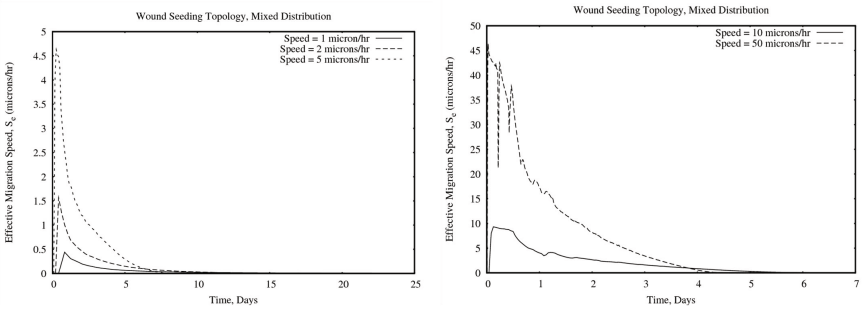

(a) (b)

Fig. 9. Effect of cell motility on the overall migration speed, S_e, of all cells inside the wound area for cell-population-1 speeds ranging from (a) 1 to $5\mu m/hr$ and (b) 10 to $50\mu m/hr$

8 Conclusion and Future Work

We described herein a three-dimensional computational model for the growth of multicellular tissues based on the concept of cellular automata to simulate wound healing. The model incorporates many aspects of cell behavior involving cell migration, division, collision, and aggregation while including multiple cell types. We presented simulation results from the serial implementation of the model using a mixed wound-seeding distribution showing the effect of varying cell migration speed of one cell population on the tissue growth rate and wound-healing time. Our simulation results indicate that increasing cell migration speeds leads to a sharp decrease in wound-healing time and that this improvement continues unabated even for larger cell speeds reaching $50\mu m/hr$. Further, our performance results point to the need for using parallel systems such as shared-memory and heterogeneous architectures, including multicore CPU

and GPU machines to run the model with much larger cellular grids in order to simulate tissue growth for more realsitic wound sizes [19]. As part of our future work, we will also consider the use of agent-based modeling for multicellular tissue growth and wound healing [20] [21].

Acknowledgments. The author would like to acknowledge the support for this research from the Research Centre in the College of Computer & Information Sciences and the Deanship of Scientific Research at King Saud University.

References

1. Safferling, K., et al.: Wound Healing Revised: A Novel Reepithelialization Mechanism Revealed by In Vitro and In Silico Models. J. Cell Biol. **203**(4), 691–709 (2013)
2. Palsson, B.O., Bhatia, S.N.: Tissue Engineering. Pearson Prentice Hall, Upper Saddle River (2004)
3. Soll, D., Wessels, D.: Motion Analysis of Living Cells: Techniques in Modern Biomedical Microscopy. Wiley-Liss, New York (1998)
4. Langer, R., Vacanti, J.P.: Tissue Engineering. Science **260**, 920–926 (1993)
5. Ben Youssef, B.: A Visualization Tool of 3-D Time-Varying Data for the Simulation of Tissue Growth. Multimed. Tools Appl. **73**(3), 1795–1817 (2014)
6. Tchuente, M.: Computation on Automata Networks. In: Soulie, F.G., Robert, Y., Tchuente, M. (eds.) Automata Networks in Computer Science: Theory and Applications, pp. 101–129. Princeton University Press, Princeton (1987)
7. Deutsch, A., Dormann, S.: Cellular Automaton Modeling of Biological Pattern Formation: Characterization, Applications, and Analysis. Birkhauser, Boston (2005)
8. Chopard, B., Droz, M.: Cellular Automata Modeling of Physical Systems. Cambridge University Press, Cambridge (1998)
9. Chang, L., Gilbert, E.S., Eliashberg, N., Keasling, J.D.: A Three-Dimensional, Stochastic Simulation of Biofilm Growth and Transport-Related Factors that Affect Structure. Micro-biology **149**(10), 2859–2871 (2003)
10. Kansal, A.R., Torquato, S., Harsh IV, G.R., Chiocca, E.A., Deisboeck, T.S.: Simulated Brain Tumor Growth Dynamics Using a Three-Dimensional Cellular Automaton. J. Theor. Biol. **203**(4), 367–382 (2000)
11. Cickovski, T.M., et al.: A Framework for Three-Dimensional Simulation of Morphogenesis. IEEE ACM T. Comput. Biol. Bioinformatics **2**(4), 273–288 (2005)
12. Schaller, G., Meyer-Hermann, M.: Multicellular Tumor Spheroid in an Off-Lattice Voronoi-Delaunay Cell Model. Phys. Rev. E **71**(5 pt. 1), 051910 (2005)
13. Beyer, T., Meyer-Hermann, M.: Delauny Object Dynamics for Tissues Involving Highly Motile Cells. In: Chauviere, A., Preziosi, L., Verdier, C. (eds.) Cell Mechanics: From Single Scale-Based Models to Multiscale Modeling, pp. 417–442. CRC Press (2010)
14. Fu, Y.X., Chaplin, D.D.: Development and Maturation of Secondary Lymphoid Tissues. Annu. Rev. Immunol. **17**, 399–433 (1999)
15. Beyer, T., Schaller, G., Deutsch, A., Meyer-Hermann, M.: Parallel Dynamic and Kinetic Regular Triangulation in Three Dimensions. Comput. Phys. Commun. **172**(2), 86–108 (2005)

16. Cordelia, Z., Mi, Q., An, G., Vodovotz, Y.: Computational Modeling of Inflammation and Wound Healing. Adv. Wound Care **2**(9), 527–537 (2013)
17. Bratley, P., Fox, B.L., Schrage, L.E.: A Guide to Simulation, 2nd edn. Springer, New York (1987)
18. Majno, G., Joris, I.: Cells, Tissues, and Disease: Principles of General Pathology. Oxford University Press, New York (2004)
19. Ben Youssef, B.: A Parallel Cellular Automata Algorithm for the Deterministic Simulation of 3-D Multicellular Tissue Growth. Cluster Comput. (2015). doi:10.1007/s10586-015-0455-7
20. An, G., Mi, Q., Dutta-Moscato, J., Vodovotz, Y.: Agent-Based Models in Translational Systems Biology. Wiley Interdiscip. Rev. **1**(2), 159–171 (2009)
21. Azuaje, F.: Computational Discrete Models of Tissue Growth and Regeneration. Brief. Bioinforma. **12**(1), 64–77 (2011)